

pubs.acs.org/JACS Article

Self-Assembly of Glycerol-Amphiphilic Janus Dendrimers Amplifies and Indicates Principles for the Selection of Stereochemistry by Biological Membranes

Dapeng Zhang, Qi Xiao, Mehrnoush Rahimzadeh, Matthew Liu, Cesar Rodriguez-Emmenegger, Yusuke Miyazaki, Wataru Shinoda, and Virgil Percec*



Cite This: J. Am. Chem. Soc. 2023, 145, 4311–4323



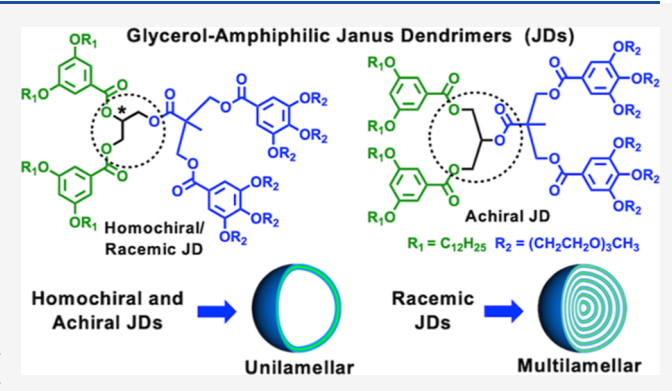
ACCESS I

III Metrics & More

Article Recommendations

Supporting Information

ABSTRACT: The principles for the selection of the stereochemistry of phospholipids of biological membranes remain unclear and continue to be debated. Therefore, any new experiments on this topic may help progress in this field. To address this question, three libraries of constitutional isomeric glycerol-amphiphilic Janus dendrimers (JDs) with nonsymmetric homochiral, racemic, and symmetric achiral branching points were synthesized by an orthogonal—modular—convergent methodology. These JDs amplify self-assembly, and therefore, monodisperse vesicles known as dendrimersomes (DSs) with predictable dimensions programmed by JD concentration were assembled by rapid injection of their ethanol solution into water. DSs of homochiral JD enantiomers, racemic, including mixtures of



different enantiomers, and achiral exhibited similar DS size-concentration dependence. However, the number of bilayers of DSs assembled from homochiral, achiral, and racemic JDs determined by cryo-TEM were different. Statistical analysis of the number of bilayers and coarse-grained molecular dynamics simulations demonstrated that homochiral JDs formed predominantly unilamellar DSs. Symmetric achiral JDs assembled only unilamellar DSs while racemic JDs favored multilamellar DSs. Since cell membranes are unilamellar, these results indicate a new rationale for nonsymmetric homochiral *vs* racemic selection. Simultaneously, these experiments imply that the symmetric achiral lipids forming more stable membrane, probably had been the preferable assemblies of prebiotic cell membranes.

INTRODUCTION

Homochirality is an essential signature of living matter. During the evolution of life, nature selected homochirality for most biological molecules and macromolecules. L-Amino acids and D-sugars have been selected as the main components of biological systems. However, phospholipids, the backbone of biological membranes, display different chirality in different living systems.³ Natural phospholipids are almost ubiquitously homochiral. Nevertheless, a case of dual homochirality is also known for phospholipids. In detail, membranes of archaea are based on sn-glycerol-1-phosphate (G1P) enantiomers with S configurational stereochemistry, while membranes of bacteria and eukaryotes employ exclusively sn-glycerol-3-phosphate (G3P) enantiomers with R configurational stereochemistry. 3a,c,4 G1P and G3P exhibit opposite handedness, but both of them provide efficient membranes. The phenomenon that different phospholipid homochiralities exist in nature is known as the lipid divide. It is believed that archaea and bacteria which are the two basal domains of life as well as eukarya have a common ancestor, referred to as the last universal common ancestor (LUCA).3,

However, the chirality of the LUCA's membrane (homochiral or heterochiral) and how G1P and G3P evolve from the LUCA's membrane remain unknown, although many theories and hypotheses toward these issues have been advanced. One theory pointed out that the LUCA's membrane was heterochiral or racemic, and the instability between the two phospholipid enantiomers eventually resulted in the lipid divide. Nevertheless, a recent study found that the robustness of cells with a hybrid heterochiral lipid membrane is higher than that with a homochiral lipid membrane. Another theory stated that the LUCA's membrane could be homochiral as it was enzymatically synthesized. However, the controversial question is what homochirality was LUCA's membrane? G1P

Received: January 11, 2023 Published: February 7, 2023





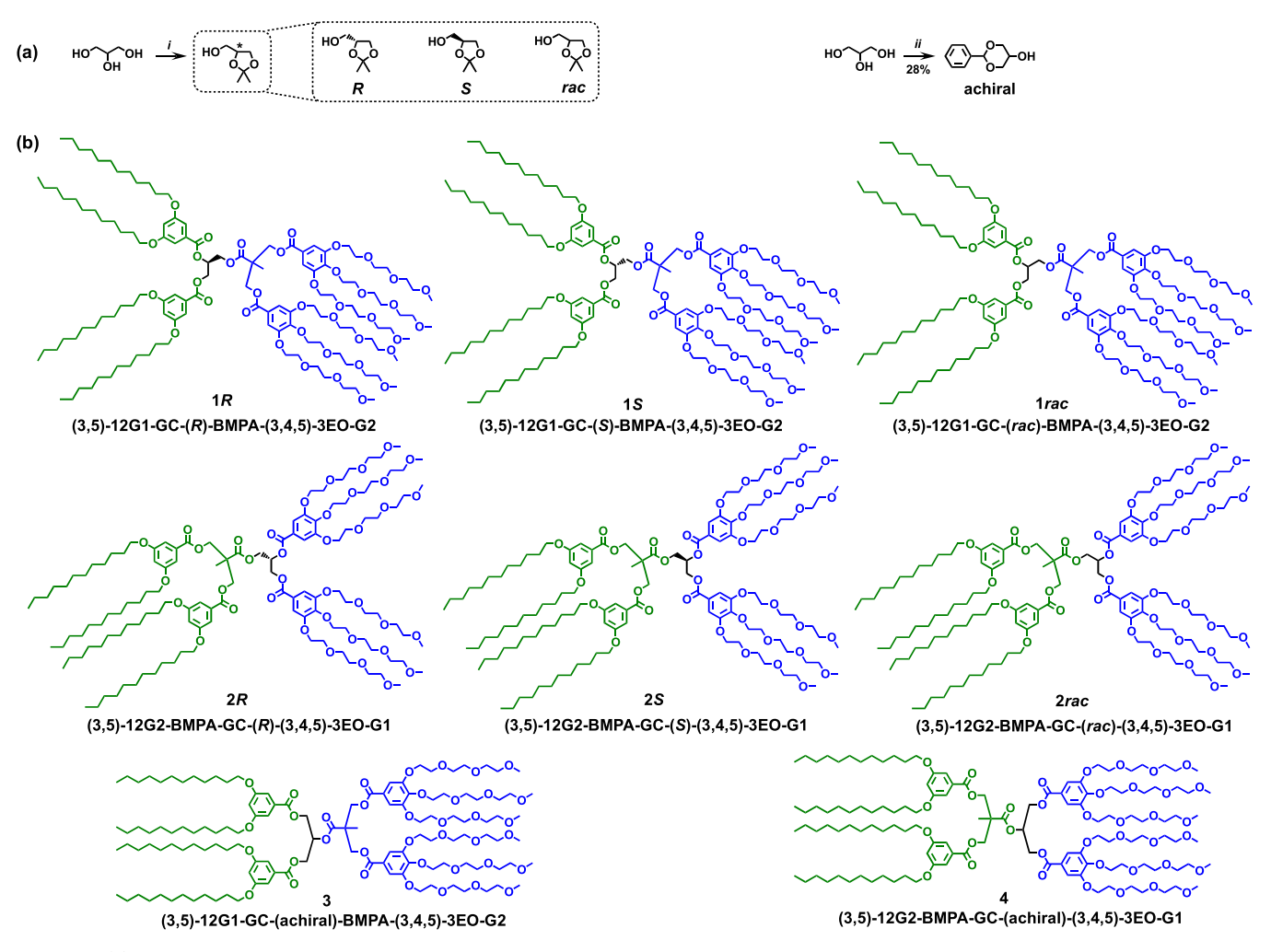


Figure 1. (a) Synthesis and nonsymmetric structures of *R*-, *S*-, and *rac*- and symmetric achiral glycerols with two protected OH. Reagents and conditions: (i) PTSA·H₂O, 4 Å MS, hexane/acetone, Dean-Stark, reflux, and 12 h and (ii) benzaldehyde, H₂SO₄, toluene, Dean-Stark, reflux, and 6 h. (b) Structures of nonsymmetric homochiral (1*R*, 1*S*, 2*R*, and 2*S*) and racemic (1*rac* and 2*rac*) and symmetric achiral (3 and 4) glycerol JDs.

or G3P? According to the literature results, both of them have been proposed and supported by different research groups. 4,5c In addition to homochiral or heterochiral possibilities, the LUCA's membrane could also be achiral. We hypothesize that the LUCA's membrane may be composed of achiral lipids, but they disappeared during the evolution of cellular life. This is probably due to the appearance of homochiral proteins including enzymes for the synthesis of membrane lipids and membrane proteins, resulting in the selectivity of homochiral lipids in biological membranes and only one chirality of lipids existing in one type of membranes.

Liposomes, an important class of biological assemblies, represent the basis of cell membranes. Synthetic variants, including synthetic liposomes, stealth liposomes, and polymersomes, have been elaborated to mimic natural cells. In addition to being models for biological membranes, synthetic liposomes and vesicles have been used to deliver active agents such as drugs and genes in vitro and in vivo. Liposomes assembled from phospholipids are unstable because the alkene units in the hydrophobic tails are readily oxidized and exhibit poor mechanical properties. Stealth liposomes coassembled from phospholipids, phospholipids conjugated with poly(ethylene glycol) (PEG) and cholesterol, are more stable but are polydisperse requiring time-consuming fractionation to desirable dimensions and narrow polydispersity. Polymersomes

assembled from amphiphilic block copolymers exhibit excellent stability but are not always biocompatible, and their membrane thickness is wider than that of cell membranes. 8

Our laboratory developed a class of vesicles named dendrimersomes (DSs), which are assembled from amphiphilic Janus dendrimers (JDs). 10 DSs exhibit better stability in time than liposomes, can be functionalized on their surface through their multivalency both in the hydrophilic and hydrophobic parts of JDs, and display similar membrane thickness.¹¹ Amphiphilic JDs with sugars conjugated on their hydrophilic part denoted Janus glycodendrimers (JGDs) self-assemble into vesicles known as glycodendrimersomes (GDSs), which mimic the glycan of biological membranes and bind sugar-binding proteins. 12 Recently, our group developed a new class of JDs, ionizable amphiphilic Janus dendrimers (IAJDs), which showed great potential in targeted delivery of messenger RNA (mRNA) in vitro and in vivo. 13 As a new synthetic delivery vector with high transfection efficiency of mRNA and high stability, IAJD facilitates the development of new mRNA vaccines and drugs. DSs are generally assembled by injection of their JD prepared in a water-miscible solvent solution such as ethanol or THF into water or buffer. This simple selfassembling procedure provides monodisperse, impermeable, and stable vesicles with excellent mechanical properties.

Scheme 1. Synthesis of Nonsymmetric Glycerol JDs of Library 1^a

"Reagents and conditions: (i) DCC, DPTS, DCM, 23 °C, and 12 h; (ii) H₂, Pd/C, EtOAc, 23 °C, and 8 h; and (iii) 1 M HCl, MeOH, 23 °C, and 1 h.

Scheme 2. Synthesis of Nonsymmetric Glycerol JDs of Library 2^a

R₁0 O HO OBn
$$I_{1}$$
 OBn I_{2} OBn I_{3} OBn I_{4} O OBn I_{4} OBn I_{5} OBn

"Reagents and conditions: (i) DCC, DPTS, DCM, 23 °C, and 12 h; (ii) H₂, Pd/C, EtOAc, 23 °C, and 8 h; and (iii) 1 M HCl, 1,4-dioxane, 60 °C, and 8 h.

The properties of DSs rely on the architecture of the assembling amphiphilic JDs. JDs assembling DSs were classified into "Twin-Twin" and "Single-Single." "Twin-Twin" JDs are constructed by combinations of twin-hydrophobic and twin-hydrophilic dendrons with an achiral pentaerythritol (PE) or tris(hydroxymethyl)aminomethane (Tris) core, while "Single-Single" JDs are made from single-hydrophobic and single-hydrophilic dendrons connected by an ester or an amide linker. Unilamellar and onion-like DSs have been discovered and designed, and their dimensions are predicted 10f by self-assembly of "Twin-Twin" and "Single-Single" JDs. 14 However, there is no report on amphiphilic JDs

with a chiral, racemic, or achiral glycerol core connecting hydrophilic and hydrophobic parts. Nature selects homochiral rather than racemic but not achiral glycerol phospholipids to construct biological membranes. In this publication, we address the very simple question: Why homochiral and not racemic or achiral lipids are used by contemporary cell membranes in biology? Only because they are enzymatically produced? What is the difference between the prebiotic primitive achiral lipids forming biological membranes and their contemporary chiral lipids?

Scheme 3. Synthesis of Symmetric Achiral Glycerol JD 3^a

^aReagents and conditions: (i) PTSA·H₂O, 2,2-dimethoxypropane, acetone, 23 °C, and 3 h; (ii) DCC, DPTS, DCM, 23 °C, and 12 h; (iii) H₂, Pd/ C, EtOAc, 23 °C, and 8 h; and (iv) 1 M HCl, 1,4-dioxane, 60 °C, and 8 h.

Scheme 4. Synthesis of Symmetric Achiral Glycerol JD 4^a

^aReagents and conditions: (i) DCC, DPTS, DCM, 23 °C, and 12 h and (ii) 1 M HCl, MeOH, 23 °C, and 1 h.

RESULTS AND DISCUSSION

Orthogonal Modular Convergent Synthesis of Three Libraries of Homochiral, Racemic, and Achiral Glycerol-Based JDs. To address the question of biological homochirality of cell membranes, we investigated the self-assembly of all constitutional isomeric glycerol JDs that facilitate the construction of homochiral, racemic, both nonsymmetric, and achiral, symmetric, structures via the stereochemistry of their branching point (Figure 1a). These JDs were expected to provide an amplification of the principles employed by phospholipids during their self-assembly and during the selection of their homochirality. Eight JDs including four homochiral, two racemic, and two achiral were synthesized (Figure 1b). Injection of their ethanol solution into water produced DSs with different dimensions and morphologies. They were characterized by dynamics light scattering (DLS) and cryogenic transmission electron microscopy (cryo-TEM).

The three libraries of glycerol-based JDs synthesized by an orthogonal-modular-convergent methodology are shown in Figure 1a,b. Both libraries 1 (top of Figure 1b) and 2 (middle of Figure 1b) contain two JDs with a nonsymmetric homochiral glycerol branching point 1R, 1S in library 1 and

2R, 2S in library 2, and one JD with a racemic branching point per library 1rac, 2rac (Figure 1b). Library 3 contains two constitutional isomeric symmetric achiral glycerol JDs (bottom of Figure 1b). The main building blocks employed in the orthogonal-modular-convergent synthesis include the hydrophilic acid 5 (Scheme 1), the hydrophilic second-generation acid 7 (Scheme 1), the hydrophobic acid 10 (Scheme 2), the hydrophobic second-generation acid 12 (Scheme 2), the R/S/rac-2,2-dimethyl-1,3-dioxolane-4-methanol (isopropylidene glycerol) containing the stereocenters, and the achiral 5hydroxy-2-phenyl-1,3-dioxane (Figure 1a and Scheme 3).

The hydrophilic acid 5 was synthesized by introducing triethylene glycol monomethyl ether in the 3,4,5-positions of the methyl ester of gallic acid, followed by hydrolysis of the ester group (Scheme S1). Two hydrophilic acids 5 were esterified by a 2,2-bis(hydroxylmethyl)propionate linker to provide the hydrophilic second-generation acid 7 (Scheme 1). Similarly, the hydrophobic acid 10 was synthesized by attaching dodecyl groups on the 3,5-positions of 3,5dihydroxybenzoic acid. 10g The hydrophobic second-generation acid 12 was prepared by connecting two hydrophobic acids 10 with a 2,2-bis(hydroxylmethyl)propionate linker (Scheme 2).

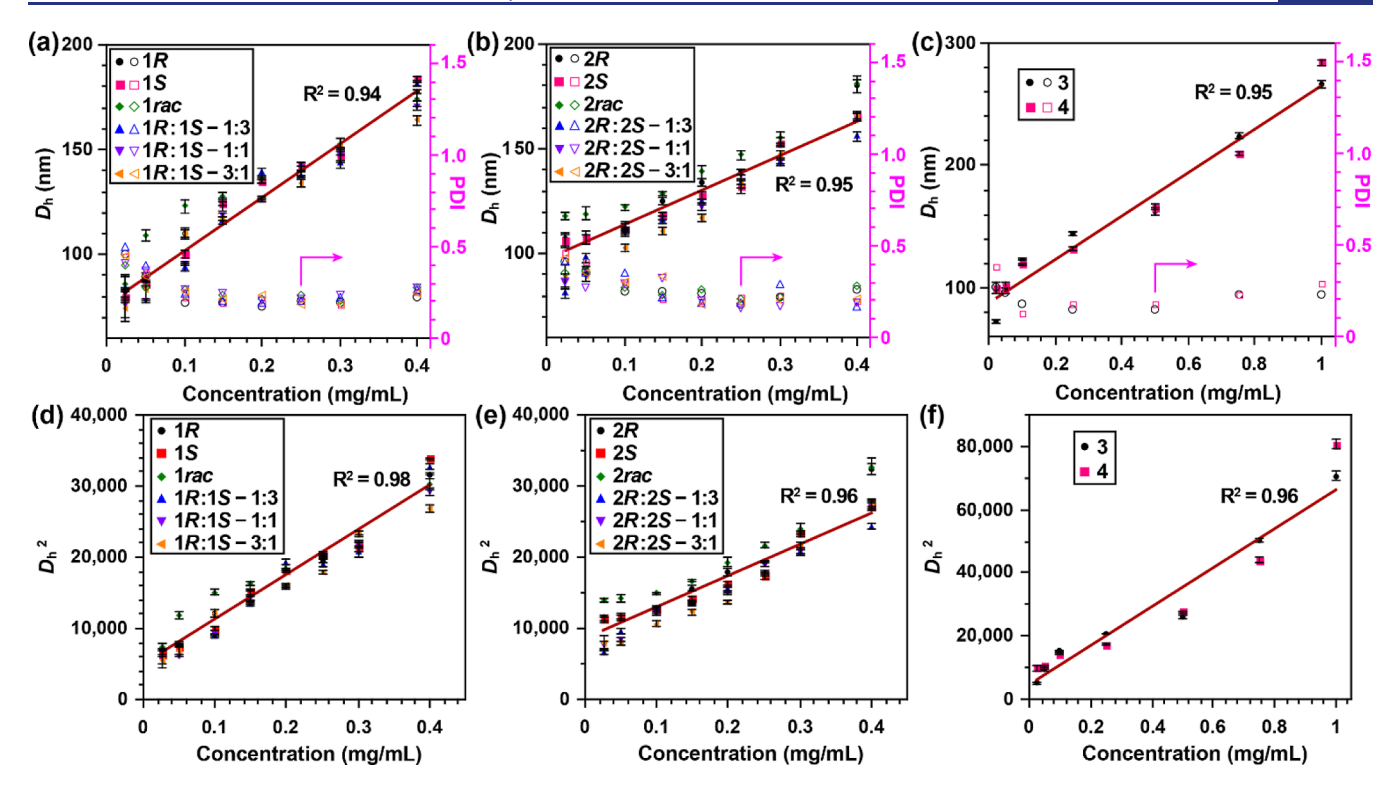


Figure 2. Concentration dependence of diameter $(D_h$, in nm) and square diameter (D_h^2) of DSs assembled by nonsymmetric and symmetric glycerol JDs in water. (a,d) Correspond to glycerol JDs of library 1. (b,e) Correspond to glycerol JDs of library 2. (c,f) Correspond to achiral glycerol JDs 3 and 4.

Table 1. Dimensions of Assemblies from Nonsymmetric Glycerol JDs in Library 1 at Different Concentrations of JDs in Water (Size Distribution Is Recorded with Intensity; Sample Number N = 3 for Each Group)

	1 <i>R</i>		18		1rac		1R:1S—1:3		1R:1S—1:1		1R:1S—3:1	
concentration of JD $(mg \cdot mL^{-1})$	D _h (nm)	PDI										
0.5	233 ± 4	0.326	229 ± 5	0.438	281 ± 3	0.240	179 ± 2	0.421	184 ± 1	0.271	266 ± 3	0.376
0.4	178 ± 1	0.228	184 ± 1	0.258	174 ± 3	0.275	181 ± 1	0.268	171 ± 2	0.274	164 ± 2	0.246
0.3	148 ± 1	0.190	147 ± 3	0.186	153 ± 2	0.203	144 ± 3	0.226	147 ± 2	0.236	153 ± 2	0.180
0.25	140 ± 2	0.202	142 ± 2	0.203	142 ± 2	0.238	138 ± 1	0.207	143 ± 1	0.214	134 ± 2	0.186
0.2	135 ± 1	0.175	135 ± 1	0.195	136 ± 2	0.216	139 ± 2	0.197	126 ± 1	0.201	127 ± 1	0.234
0.15	124 ± 1	0.195	124 ± 3	0.190	128 ± 2	0.232	116 ± 2	0.206	119 ± 1	0.247	117 ± 1	0.210
0.1	110 ± 3	0.197	100 ± 2	0.223	123 ± 3	0.268	94 ± 2	0.243	96 ± 1	0.269	110 ± 2	0.257
0.05	87 ± 2	0.336	86 ± 1	0.359	109 ± 3	0.277	89 ± 2	0.401	78 ± 1	0.368	83 ± 5	0.334
0.025	82 ± 2	0.455	80 ± 3	0.446	86 ± 4	0.398	84 ± 5	0.502	76 ± 8	0.410	74 ± 4	0.451

Table 2. Dimensions of Assemblies from Nonsymmetric Glycerol JDs in Library 2 at Different Concentrations of JDs in Water (Size Distribution Is Recorded with Intensity; Sample Number N = 3 for Each Group)

	2R		28		2rac		2R:2S—1:3		2R:2S—1:1		2R:2S —3:1	
concentration of JD $(mg \cdot mL^{-1})$	D _h (nm)	PDI										
0.5	319 ± 4	0.497	288 ± 5	0.295	412 ± 13	0.449	304 ± 3	0.511	324 ± 6	0.452	390 ± 10	0.371
0.4	180 ± 3	0.263	165 ± 2	0.205	181 ± 4	0.283	156 ± 2	0.170	165 ± 2	0.195	166 ± 2	0.218
0.3	152 ± 1	0.227	153 ± 2	0.235	155 ± 3	0.225	144 ± 2	0.295	144 ± 1	0.175	147 ± 2	0.208
0.25	139 ± 1	0.186	132 ± 3	0.223	147 ± 2	0.211	134 ± 1	0.192	138 ± 2	0.158	133 ± 2	0.193
0.2	134 ± 2	0.242	128 ± 2	0.203	139 ± 3	0.260	125 ± 1	0.189	122 ± 1	0.205	117 ± 2	0.188
0.15	125 ± 2	0.257	119 ± 1	0.212	129 ± 1	0.236	116 ± 2	0.223	117 ± 1	0.324	111 ± 2	0.335
0.1	111 ± 2	0.258	112 ± 2	0.291	122 ± 1	0.277	113 ± 2	0.359	110 ± 2	0.293	103 ± 2	0.305
0.05	108 ± 3	0.368	107 ± 2	0.422	119 ± 3	0.365	98 ± 2	0.359	92 ± 2	0.280	89 ± 2	0.361
0.025	107 ± 3	0.416	106 ± 3	0.465	118 ± 2	0.361	81 ± 2	0.419	87 ± 3	0.309	89 ± 6	0.439

For library 1 (Scheme 1), the hydrophilic second-generation acid 7 was reacted with rac/R/S-2,2-dimethyl-1,3-dioxolane-4-

methanol, followed by deprotection to generate the corresponding diol 9. The esterification of this hydrophilic diol and

two hydrophobic first-generation acids produced 1R, 1S, and 1rac in 75–86% isolated yield.

The synthesis of 2R, 2S, and 2rac of library 2 (Scheme 2) was accomplished by the esterification performed with the hydrophobic second-generation acid and the second esterification with the hydrophobic diol 14 and two hydrophilic acids 5 in 73–78% isolated yield. Schemes 3 and 4 outline the synthesis of the achiral JDs 3 and 4. The achiral branching core 17 was synthesized by the esterification of 16 with 5-hydroxy-2-phenyl-1,3-dioxane to produce diol 18 after deprotection of the benzylidene acetal group. The achiral JDs 3 and 4 were synthesized by attaching two hydrophilic acids 5 and two hydrophobic acids 10 to diol 18 (Schemes 3 and 4). The detailed synthesis and characterization are available in the Supporting Information.

Self-Assembly of Glycerol JDs into DSs. The self-assembly of all eight glycerol JDs was performed by injection of their ethanol solution (50 μ L) into 1 mL of Milli-Q water. DSs are kinetically controlled assemblies. The size distribution and structure of the resulting DSs were analyzed by DLS (Figure 2) and cryo-TEM. Previously, we found that unilamellar and onion-like DSs assembled from "Twin–Twin" and "Single–Single" JDs displayed a size-concentration dependence. In a certain concentration range, the size of DSs increased with the concentration of JDs injected in water or buffer. A similar size-concentration dependence was observed for glycerol JDs (Figure 2). The detailed experimental results are summarized in Tables 1–3, and representative DLS curves are shown in

Table 3. Dimensions of Assemblies from Symmetric Achiral Glycerol JDs 3 and 4 at Different Concentrations of JDs in Water (Size Distribution Is Recorded with Intensity; Sample Number N = 3 for Each JD)

	3		4		
concentration of JD $(mg \cdot mL^{-1})$	D _h (nm)	PDI	D _h (nm)	PDI	
1.0	266 ± 3	0.233	284 ± 3	0.291	
0.75	224 ± 2	0.236	210 ± 2	0.233	
0.5	162 ± 3	0.152	166 ± 2	0.183	
0.25	144 ± 1	0.153	132 ± 2	0.180	
0.1	123 ± 1	0.183	119 ± 1	0.136	
0.05	97 ± 2	0.241	102 ± 2	0.266	
0.025	72 ± 2	0.272	100 ± 5	0.391	

Figure 3. The derived count rates of all DSs are between 150 and 500 kilo counts per second (kcps). Figure 2a shows how

the size of the resulting DSs increased with the concentration of JDs in water for 1R, 1S, and 1rac for concentration range from 0.025 to 0.5 mg·mL⁻¹. The dimensions of the assemblies were identical when the concentrations of the JDs in water were identical, and the linear fitting line of the sizeconcentration dependence represented this identical trend. Sizes of assemblies from mixtures of 1R and 1S in different ratios (1:3, 1:1, and 3:1) were also identical (Figure 2a). This indicated that sizes of assemblies from JD homochiral enantiomers (1R and 1S) and racemic mixtures with different ratios of enantiomers were identical at the same concentrations of JDs in water. This is expected since, with the exception of the rotation of polarized light, the physical properties of enantiomers and of their racemic mixtures must be identical. In addition, the square of the diameter of DSs displayed a linear dependence on concentration in the range from 0.025 to 0.4 for homochiral and racemic and to 1.0 mg·mL⁻¹ for achiral JDs (Figure 2d,f). This result is consistent with the sizeconcentration relationship of JDs already reported 106,14b and helps predict the dimensions of DSs with the aid of JD concentrations.

2R, **2S**, and **2rac** as well as mixtures of **2R** and **2S** with different molar ratios (1:3, 1:1, and 3:1) showed a similar size-concentration dependence (Figure 2b). The diameter rather than the square of diameter of DSs displayed a linear relationship vs concentration of glycerol JD in the concentration range from 0.025 to 0.4 for homochiral and racemic and to 1.0 mg·mL⁻¹ for achiral JDs (Figure 2b,c,e). In addition, the representative dependence of polydispersity index (PDI) on diameter (D_h , in nm) for DSs assembled by glycerol JDs **1R**, **2R**, and **3** is shown in Figure 4, in which we can see when the sizes of DSs are larger than 120 nm, the PDI is smaller than 0.3, while the PDI increases to around 0.4 when the sizes are smaller than 120 nm, which may result in the deviation of linear size-concentration dependence when the concentration of JDs is lower than 0.1 mg·mL⁻¹.

Determination of the Structure of Homochiral, Racemic, and Achiral DSs by Cryo-TEM. Although dimensions do not show differences when comparing homochiral, achiral, and racemic JDs, the structure of the resulting DSs was investigated by cryo-TEM. Substantial differences were observed during cryo-TEM investigations. cryo-TEM of enantiomers 2R and 2S (Figure 5a,b) showed unilamellar DSs predominantly, being accompanied by a small amount of multilamellar DSs. The cryo-TEM images of glycerol JD 2rac (Figure 5c) showed the opposite result, in

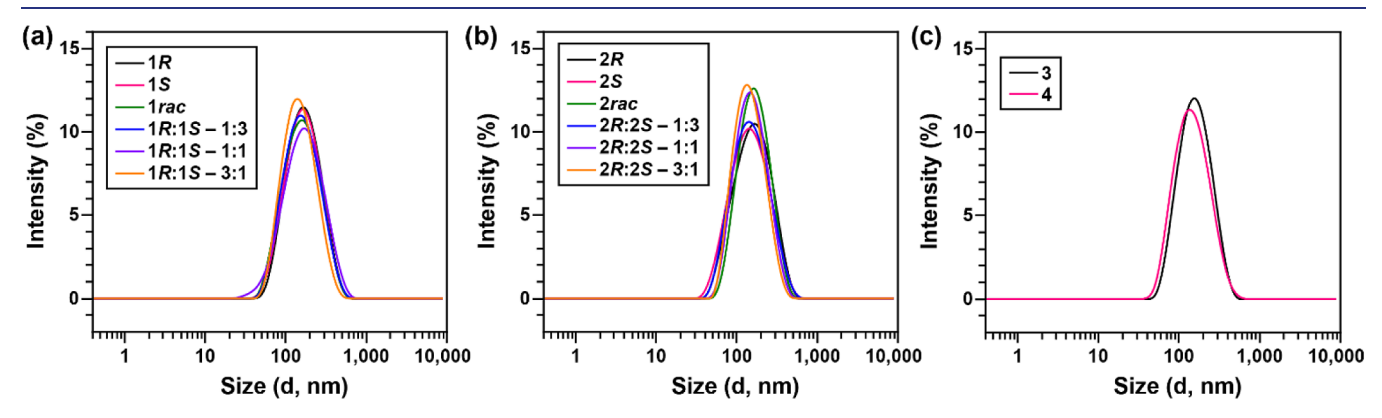


Figure 3. Representative DLS curves of assemblies from glycerol JDs in library 1 (a), library 2 (b), and achiral JDs 3 and 4 (c) with the same concentration of JD $(0.25 \text{ mg}\cdot\text{mL}^{-1})$ in water (size distribution is recorded with intensity).

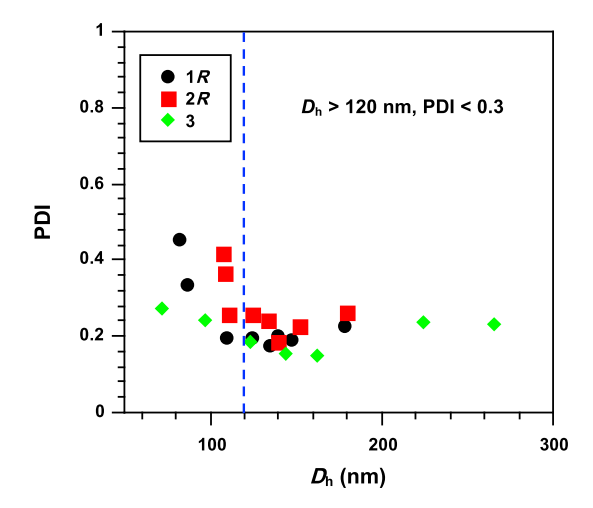


Figure 4. Dependence of PDI on diameter ($D_{\rm h}$, in nm) for DSs assembled by glycerol JDs **1R**, **2R**, and **3**. All DSs show a PDI lower than 0.3 when the corresponding $D_{\rm h}$ is larger than 120 nm.

which multilamellar DSs were predominant while unilamellar DSs were observed in a small amount. The red numbers in Figure 5 stand for the unilamellar DSs, while the yellow numbers for multilamellar DSs. The calculated percentages of unilamellar DSs in the selected images for 2R, 2S, and 2rac are 91% (11 DSs counted), 70% (40 DSs counted), and 13% (48 DSs counted), respectively. The same trend was found for cryo-TEM of 1R, 1S, and 1rac (Figures S23–S25). This indicates that homochiral JDs tend to self-assemble predominantly into unilamellar DSs, while racemic favor the formation of multilamellar DSs. Achiral DSs from glycerol JDs 3 and 4 are all unilamellar (Figures 5d–f and S29 and S30). In

addition, the 3D surface plots of vesicles in the corresponding cryo-TEM images further prove this phenomenon. As shown in Figure 6a—d, homochiral JDs 1R, 1S, 2R, and 2S self-assemble into unilamellar DSs, while racemic JDs 1rac and 2rac self-assemble into onion-like multilamellar DSs (Figure 6e—g). Achiral JDs 3 and 4 self-assemble into unilamellar DSs (Figure 6h,i), which is similar to homochiral JDs, but they exhibit more solid membranes compared to those assembled by 1R, 1S, 2R, and 2S JDs.

Statistical Analysis of the Structure of Homochiral, Racemic, and Achiral DSs. Statistical analysis was used to organize the number of bilayers from cryo-TEM. The distribution of the number of lamellae in DSs was analyzed for each sample to construct the respective histograms (Figure 7). The histograms represent the distribution function of probability. The number of bilayers of racemic JDs (1rac and 2rac) exhibit a near-normal distribution (Gaussian) as demonstrated by various statistic tests. However, the enantiomerically pure JDs (1R, 1S, 2R, and 2S) exhibit Chisquared distribution (χ^2 distribution) with a shape parameter of 1 or 2. The difference in the distributions of number of bilayers for homochiral νs racemic glycerol-based JDs emphasizes the difference between the self-assembly structures, unilamellar νs multilamellar.

To investigate the normality of the distribution of racemic JDs, we used SPSS statistics software, which utilized normality tests of Kolmogorov–Smirnov and Shapiro–Wilk. Both methods demonstrated that the distribution of racemic JDs (1rac and 2rac) were normal-like. For a more detailed study of distribution functions, we calculated the skewness (third standardized moment and a measure of the asymmetry) and kurtosis (fourth standardized moment and a measure of the extreme values in either tail) of the data (number of DS layers,

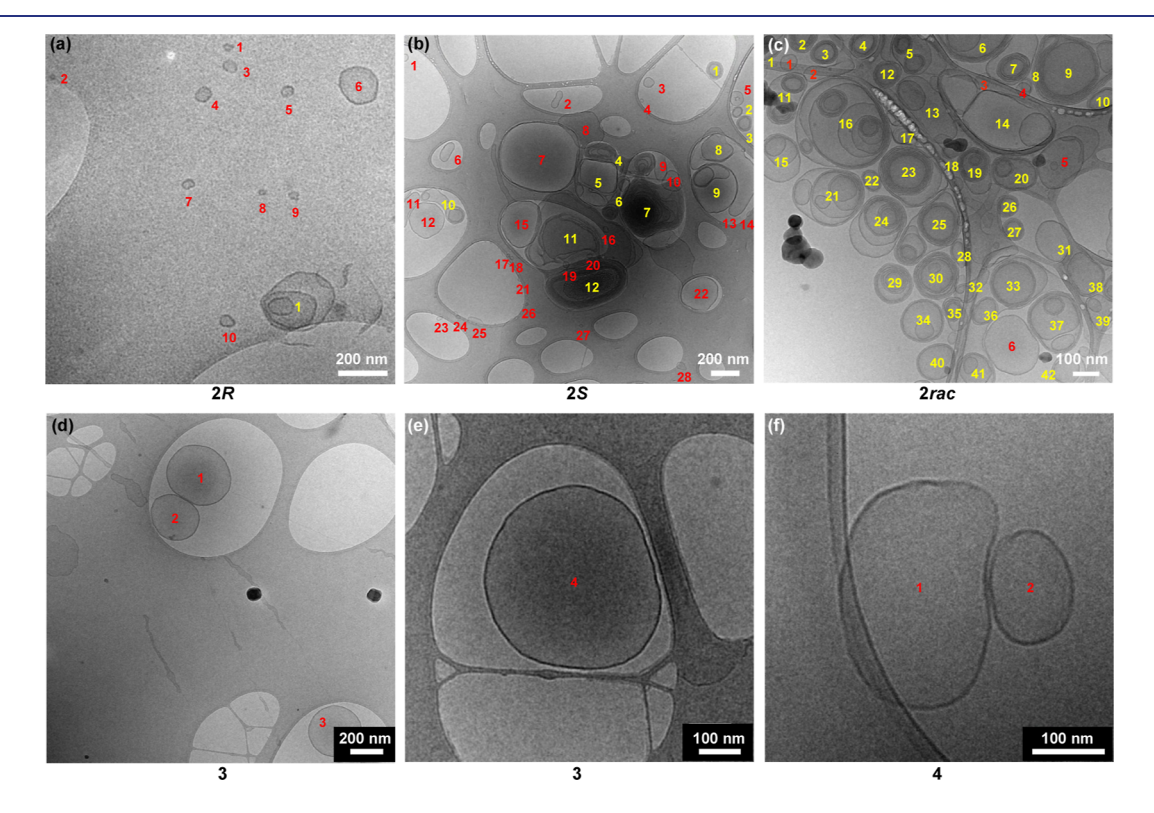


Figure 5. Selected cryo-TEM images of DSs assembled by glycerol JDs 2R (a), 2S (b), 2rac (c), achiral 3 (d,e), and achiral 4 (f). The concentration of glycerol JDs was 1 mg·mL⁻¹.

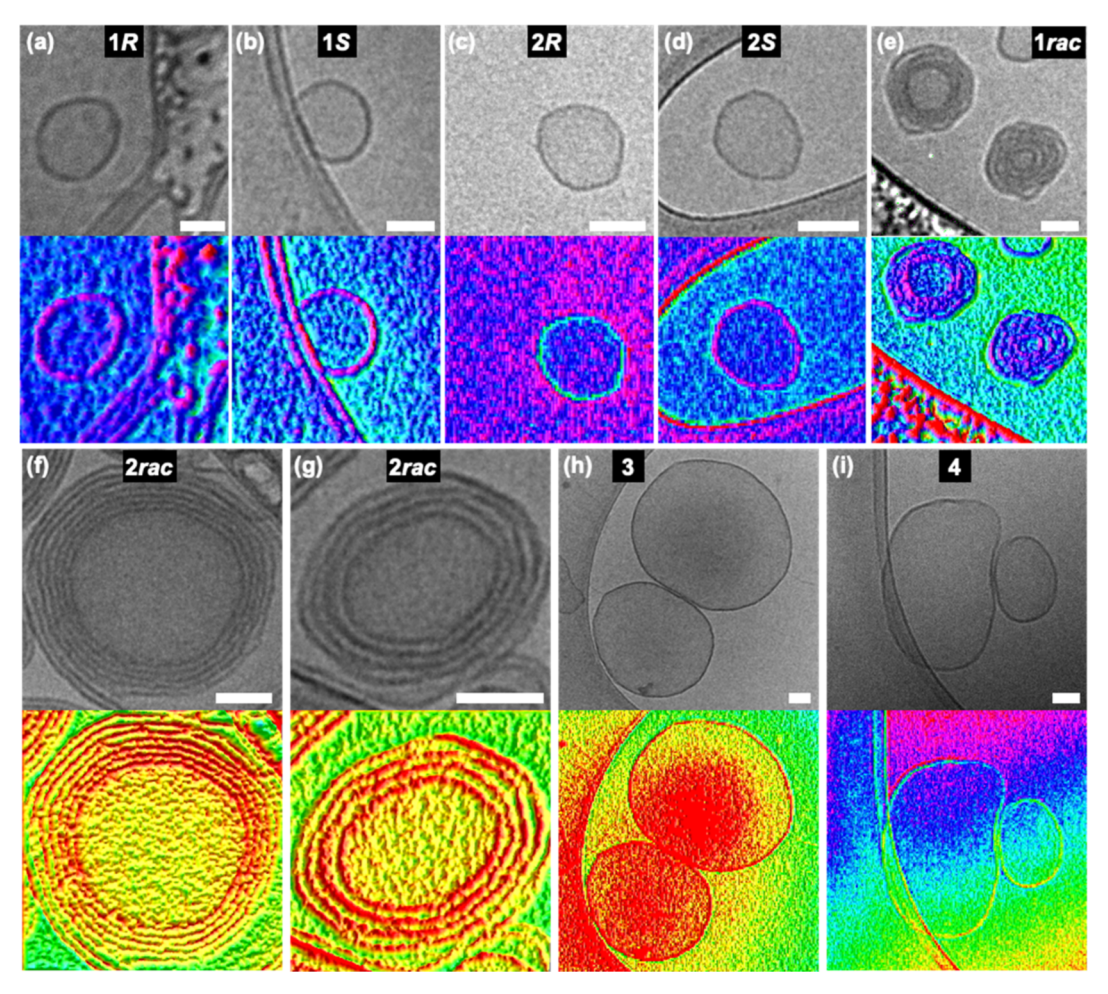


Figure 6. Representative cryo-TEM images (the upper half part in the panel) and 3D surface plots (the lower half part in the panel) of DSs assembled by glycerol JDs. (a) Corresponds to the DS assembled by 1R. (b) Corresponds to the DS assembled by 1S. (c) Corresponds to the DS assembled by 2R. (d) Corresponds to the DS assembled by 2rac. (f,g) Correspond to the DSs assembled by 2rac. (h) Corresponds to the DS assembled by 3. (i) Corresponds to the DS assembled by 4. The scale bar is 50 nm. The 3D surface plots were generated by ImageJ software through transforming the pixel values (luminance) into height information, with darker areas (lower grayscale values) corresponding to greater heights.

Tables S1 and S2). The skewness of the distributions of the number of bilayers for 1rac and 2rac is slightly positive (0.70 and 0.58, respectively). Positive skewness means the tails are extending to the right. These relatively low values are in line with the previous conclusion that their distribution is normallike. Comparing the skewness of the distribution of racemic JDs with homochiral JDs shows that 1R, 1S, 2R, and 2S are very positively skewed (1.977, 1.687, 3.313, and 3.029, respectively) and nonsymmetric. This difference in distribution parameter (skewness) strongly supports the difference between homochiral (unilamellar) and racemic (multilamellar) glycerol-based JDs.

The second distribution parameter which we have investigated is the kurtosis and excess kurtosis (kurtosis -3). For normal distribution, the kurtosis is 3, and the excess of kurtosis is zero. The distributions of racemic JDs have negative kurtosis (-1.623 for 1rac and -0.423 for 2rac), indicating that the peak is lower than the peak of a normal distribution. While homochiral JDs show distributions with positive kurtosis (3.932 for 1R, 2.797 for 1S, 10.980 for 2R, and 9.502 for 2S), indicating that the corresponding peaks are higher than those of the normal distribution. This result highlights the difference

between the number of bilayers of DSs assembled from homochiral and racemic glycerol JDs.

Coarse-Grained Molecular Dynamics Simulations of Homochiral, Racemic, and Achiral DSs. To investigate the chirality effect on the morphological and topological changes in JD aggregates, we conducted coarse-grained (CG) molecular dynamics (MD) simulations for large aggregates composed of 20,000 JD molecules using the SPICA force field. 15 The simulation protocol here is the same as that we used for vesicle formation simulation.¹⁵ First, JDs were randomly arranged in a cubic simulation box and hydrated with approximately 50 CG water particles per JD molecule (Figure 8a). Then, the JD aggregates obtained after energy minimization and 50 ns equilibration MDs were placed into a larger water box. At this stage, the CG water per JD molecule was increased to approximately 245 particles. Then, to monitor the development of morphology and topology of JD aggregates in dilute solutions, we performed 2 μ s MDs for glycerol JDs 2Rand 2rac aggregate systems, while we ran 1.5 μ s MDs for achiral JD 3 and 4 aggregates. Figure 8b displays the final configurations obtained from the MDs. The maximum radii of glycerol JDs 2R, 3, and 4 aggregates were estimated to be approximately 40 nm, which is larger than that of the JD 2rac

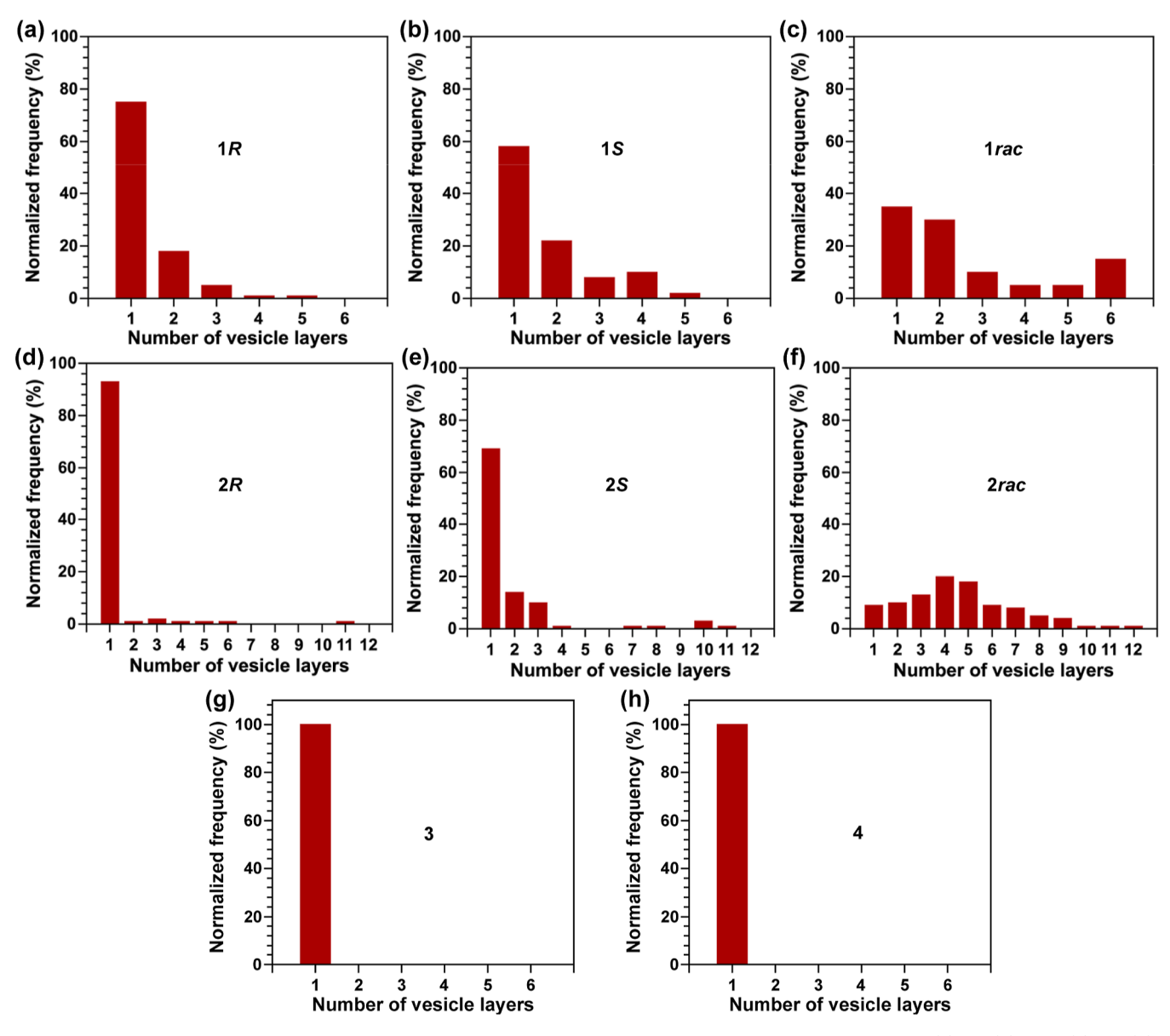


Figure 7. Histograms of the normalized frequency of number of vesicle layers of DSs assembled from glycerol JDs 1R (a), 1S (b), 1rac (c), 2R (d), 2S (e), and 2rac (f) and achiral JDs 3 (g) and 4 (h) by statistical analysis. Number of DSs counted for each glycerol JD: 82 (1R), 40 (1S), 20 (1rac), 216 (2R), 92 (2S), 306 (2rac), 10 (3), and 3 (4).

aggregate (approximately 35 nm). In addition, we characterized the target JD membrane by calculating the typical membrane properties, area per lipid, line tension, and bending modulus using the built CG model. The calculated membrane properties are listed in Table S8.

For the JD **2**rac system, the aggregate formed a more compact, onion-like structure compared to the other systems. While the JD **2**R, **3**, and **4** aggregates formed swelling regions on the outermost layer, the JD **2**rac aggregate did not form such regions and included stacked layers. These results agree well with the experimental result, which indicate that **2**rac JDs have the potential to form onion-like structures in comparison to other chiral and achiral JDs, although the other JDs could not attain complete unilamellar vesicles within the simulation time scale (even though the physical time scale of CG MD can be 10 times longer than the simulation time; which means effectively 20 μ s). Although the physical membrane properties of the JD aggregates have been explored, no significant

uniqueness of the *2rac* bilayer membrane was detected (Table S8). However, the line tensions of the achiral JDs are higher than those of the chiral JDs, which indicates that the bilayer structure of achiral JD aggregates is more stable than that of chiral JDs. This is because a high line tension can prevent water leakage through vesicular layers. This finding may also correspond to the experimental result that the achiral JDs can maintain and only form unilamellar vesicles, which are stable without multilamellar stacking.

Simulation times on the order of microseconds may not have been sufficient to relax the aggregate structure. In fact, some hydrophilic pores remained on the aggregate surface even after our simulations conducted at relatively high temperatures with glycerol JDs 2R, 3, and 4. Therefore, the aggregates in these systems may continue to grow as the simulation time is extended. The initial configuration of the simulated systems might also have affected the results obtained from the JD aggregate simulations. To investigate the stability

pubs.acs.org/JACS

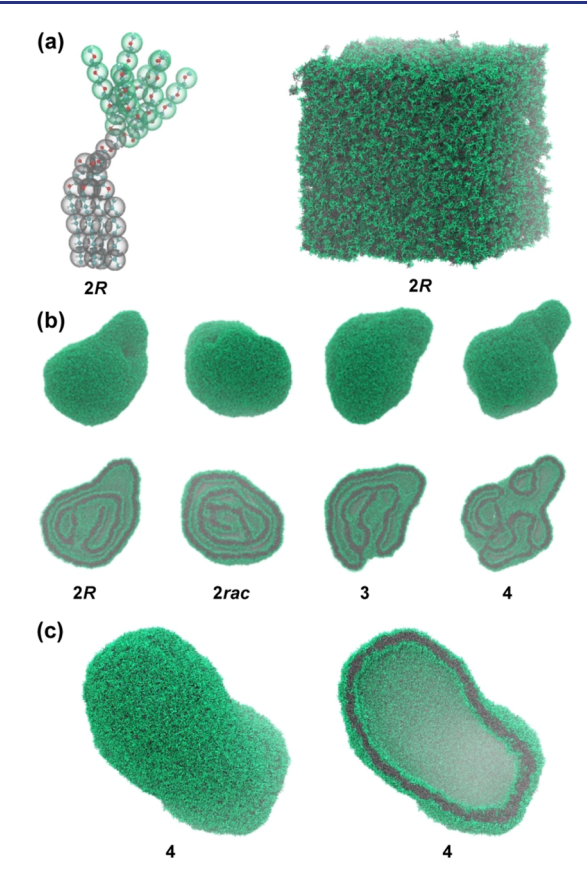


Figure 8. Simulations of DSs assembled from glycerol JDs **2R**, **2rac**, **3**, and **4**. (a) Left: coarse-grained **2R** JD structure. Right: initial configuration of the JD aggregate systems. Glycerol JD headgroups and tails are colored green and gray, respectively. Water is omitted for clarity. (b) Entire and cross-sectional views of the final configuration of microsecond-order CG MD for JD aggregates. (c) Entire (left) and cross-sectional (right) views of the final aggregate configuration in the achiral JD **4**.

of the unilamellar structure in the JD aggregate, we additionally carried out 500 ns CG MD analysis on the achiral JD 4 aggregate, through which its complicated internal structure was removed from the initial configuration provided by the previous simulation. Figure 8c shows the final configuration of the simulation. The observed unilamellar vesicle of symmetric achiral JD 4 was stable during the simulation. Pores that were presented in the initial configuration were closed quickly, and no significant morphology change of the vesicle was detected later. Thus, the CG MD simulations successfully demonstrate the apparent onion-like structure of 2rac, clear difference in the line tension between chiral and achiral JDs, and stable unilamellar structure of the JD 4 assembly, which supports the DLS and cryo-TEM experimental outcomes.

CONCLUSIONS

Glycerol JDs with nonsymmetric homochiral, symmetric achiral, and nonsymmetric racemic branching points were synthesized. They self-assemble into monodisperse DSs by simple injection of their ethanol solution into water. DLS measurements showed that the resulting DSs are concentration-size dependent with an identical trend regardless of achiral, homochiral, or racemic branching point. Therefore, DLS experiments alone cannot discriminate between the DSs

assembled from these glycerol JDs. However, cryo-TEM and statistical analysis showed that homochiral JDs form predominantly unilamellar, while racemic JDs favor multilamellar, onion-like DSs. Symmetric achiral JDs produce only unilamellar DSs. Statistical analysis of the number of bilayers showed that homochiral JDs self-assemble predominantly unilamellar, achiral only unilamellar, while racemic predominantly multilamellar, onion-like DSs. CG MD simulations displayed similar results with racemic ID 2rac showing the potential to form onion-like structures and achiral JD 4 showing a stable unilamellar structure, although homochiral JD 2R could not form complete unilamellar structures in the limited simulation time of microseconds. This study provides a rationale for the selection of homochirality of phospholipids by nature since single-bilayer membranes are required for the construction of biological cell membranes. However, it also demonstrates that symmetric achiral lipids, which were most probably available in prebiotic primitive cells, provide the most stable vesicles. 16 While the amplified structure of JDs investigated here was never part of the prebiotic or contemporary biological membranes, the results reported here may provide new hypothesis for the field of biological membranes generated from phospholipids. The less stable homochiral contemporary membranes are stabilized by transmembrane proteins, cholesterol, and glycoconjugates and thus overcome the higher stability of the prebiotic achiral primitive cells. The work reported here is complementary to that on the origins of homochirality addressed with selfassembling dendritic dipeptides¹⁷ and via deracemization in the crystal state. 18 The mechanisms explaining the formation of unilamellar DSs from homochiral and achiral JDs and the potential formation of giant unilamellar DSs by simple injection, 16d as well as the role of chirality in drug delivery including in the targeted delivery of mRNA, 13 are under investigation. Our previous research on the discovery of the self-assembly of amphiphilic JDs into multilamellar onion-like DSs^{14a} and GDSs^{14d} inspired immediate development of models to explain the onion concept by dissipative particle dynamics methods. 19 The development of a molecular model that explains the mechanism of deracemization 18 vs onion formation of racemic JDs is in progress, and it will be reported in an independent publication.

ASSOCIATED CONTENT

Solution Supporting Information

The Supporting Information is available free of charge at https://pubs.acs.org/doi/10.1021/jacs.3c00389.

Experimental methods, synthetic procedures with complete characterization data, additional cryo-TEM data, statistical analysis data, and supplemental references (PDF)

AUTHOR INFORMATION

Corresponding Author

Virgil Percec — Roy & Diana Vagelos Laboratories, Department of Chemistry, University of Pennsylvania, Philadelphia, Pennsylvania 19104-6323, United States; orcid.org/0000-0001-5926-0489; Email: percec@sas.upenn.edu

Authors

Dapeng Zhang — Roy & Diana Vagelos Laboratories,
Department of Chemistry, University of Pennsylvania,
Philadelphia, Pennsylvania 19104-6323, United States;
Present Address: Laboratory of Low-Dimensional
Materials Chemistry, School of Materials Science and
Engineering, East China University of Science and
Technology, Shanghai 200237, China; orcid.org/0000-0003-4222-6107

Qi Xiao — Roy & Diana Vagelos Laboratories, Department of Chemistry, University of Pennsylvania, Philadelphia, Pennsylvania 19104-6323, United States; Institute of Computational Molecular Science, Temple University, Philadelphia, Pennsylvania 19122, United States; Present Address: ET Healthcare, Inc. and Gator Bio, 2455 Faber Place, Palo Alto, CA 94303, United States.; orcid.org/0000-0002-6470-0407

Mehrnoush Rahimzadeh – DWI—Leibniz Institute for Interactive Materials, Aachen 52074, Germany; Institute of Technical and Macromolecular Chemistry, RWTH Aachen University, Aachen 52074, Germany

Matthew Liu — Roy & Diana Vagelos Laboratories, Department of Chemistry, University of Pennsylvania, Philadelphia, Pennsylvania 19104-6323, United States; orcid.org/0000-0002-5004-9182

Cesar Rodriguez-Emmenegger — DWI—Leibniz Institute for Interactive Materials, Aachen 52074, Germany; Institute of Technical and Macromolecular Chemistry, RWTH Aachen University, Aachen 52074, Germany; Present Address: Institute for Bioengineering of Catalonia (IBEC), The Barcelona Institute of Science and Technology (BIST), Carrer de Baldiri Reixac, 10, 12, Barcelona 08028, Spain; Institució Catalana de Recerca i Estudis Avançats (ICREA), Passeig Lluís Companys 23, Barcelona 08010, Spain.; orcid.org/0000-0003-0745-0840

Yusuke Miyazaki — Research Institute for Interdisciplinary Science, Okayama University, Okayama 700-8530, Japan Wataru Shinoda — Research Institute for Interdisciplinary Science, Okayama University, Okayama 700-8530, Japan; orcid.org/0000-0002-3388-9227

Complete contact information is available at: https://pubs.acs.org/10.1021/jacs.3c00389

Notes

The authors declare no competing financial interest.

ACKNOWLEDGMENTS

This work was supported by the National Science Foundation grants DMR-1807127 (V.P.) and DMR-1720530 (to V.P.), the P. Roy Vagelos Chair at the University of Pennsylvania (V.P.), the Alexander von Humboldt Foundation (to V.P.), the European Union's Horizon H2020-NMBP-TR-IND-2018, EVPRO (Development of Extracellular Vesicles loaded hydrogel coatings with immunomodulatory activity for Promoted Regenerative Osseo integration of revision endoprosthesis) grant 814495-2 (to C.R.-E.), and JSPS KAKENHI grant no. JP21H01880 (to W.S.). Calculations were performed at the facilities of the Research Center for Computational Science, Okazaki (project: 22-IMS-C108) and the Institute for Solid State Physics, and the University of Tokyo. We thank a reviewer for encouraging us to develop a molecular model

explaining the self-assembly of onions from racemic amphiphilic JDs.

■ REFERENCES

(1) (a) Franck, P.; Bonner, W. A.; Zare, R. N. On the One Hand but Not the Other: The Challenge of the Origin and Survival of Homochirality in Prebiotic Chemistry. In Chemistry for the 21th Century; Keinan, E., Schecter, I., Eds.; Wiley-VCH: Weinheim, 2000; pp 175-208. (b) Lehn, J.-M. From Supramolecular Chemistry Towards Constitutional Dynamic Chemistry and Adaptive Chemistry. Chem. Soc. Rev. 2007, 36, 151-160. (c) Hein, J. E.; Gherase, D.; Blackmond, D. G. Chemical and Physical Models for the Emergence of Biological Homochirality. Top. Curr. Chem. 2013, 333, 83-108. (d) Rowan, A. E.; Nolte, R. J. M. Helical Molecular Programming. Angew. Chem., Int. Ed. 1998, 37, 63-68. (e) Weissbuch, I.; Lahav, M. Crystalline Architectures as Templates of Relevance to the Origins of Homochirality. Chem. Rev. 2011, 111, 3236-3267. (f) Addadi, L.; Weiner, S. Crystals, Asymmetry and Life. Nature 2001, 411, 753-755. (g) Ziblat, R.; Leiserowitz, L.; Addadi, L. Crystalline Lipid Domains: Characterization by X-Ray Diffraction and their Relation to Biology. Angew. Chem., Int. Ed. 2011, 50, 3620-3629. (h) Pokroy, B.; Kang, S. H.; Mahadevan, L.; Aizenberg, J. Self-Organization of a Mesoscale Bristle into Ordered Hierarchichal Helical Assemblies. Science 2009, 323, 237-240. (i) Addadi, L.; Boom, M. Heroes of Stereochemistry and Crystals. Isr. J. Chem. 2021, 61, 681-682. (j) Krieg, E.; Bastings, M. M. C.; Besenius, P.; Rybtchinski, B. Supramolecular Polymers in Aqueous Media. Chem. Rev. 2016, 116, 2414-2477.

(2) (a) Kumar, A.; Capua, E.; Kesharwani, M. K.; Martin, J. M. L.; Sitbon, E.; Waldeck, D. H.; Naaman, R. Chirality-Induced Spin Polarization Places Symmetry Constraints on Biomolecular Interactions. *Proc. Natl. Acad. Sci. U.S.A.* 2017, 114, 2474–2478. (b) Yeom, J.; Guimaraes, P. P. G.; Ahn, H. M.; Jung, B.-K.; Hu, Q.; McHugh, K.; Mitchell, M. J.; Yun, C.-O.; Langer, R.; Jaklenec, A. Chiral Supraparticles for Controllable Nanomedicine. *Adv. Mater.* 2020, 32, 1903878.

(3) (a) Sojo, V. On the Biogenic Origins of Homochirality. *Origins Life Evol. Biospheres* **2015**, 45, 219–224. (b) Liu, L.; Zou, Y.; Bhattacharya, A.; Zhang, D.; Lang, S. Q.; Houk, K. N.; Devaraj, N. K. Enzyme-Free Synthesis of Natural Phospholipids in Water. *Nat. Chem.* **2020**, *12*, 1029–1034. (c) Martin, H. S.; Podolsky, K. A.; Devaraj, N. K. Probing the Role of Chirality in Phospholipid Membranes. *ChemBioChem* **2021**, *22*, 3148–3157.

(4) Coleman, G. A.; Pancost, R. D.; Williams, T. A. Investigating the Origins of Membrane Phospholipid Biosynthesis Genes Using Outgroup-Free Rooting. *Genome Biol. Evol.* **2019**, *11*, 883–898.

(5) (a) Koga, Y.; Kyuragi, T.; Nishihara, M.; Sone, N. Did Archaeal and Bacterial Cells Arise Independently from Noncellular Precursors? A Hypothesis Stating that the Advent of Membrane Phospholipid with Enantiomeric Glycerophosphate Backbones Caused the Separation of the Two Lines of Descent. J. Mol. Evol. 1998, 46, 54-63. (b) Wächtershäuser, G. From Pre-Cells to Eukarya - A Tale of Two Lipids. Mol. Microbiol. 2003, 47, 13-22. (c) Yokobori, S. I.; Nakajima, Y.; Akanuma, S.; Yamagishi, A. Birth of Archaeal Cells: Molecular Phylogenetic Analyses of G1P Dehydrogenase, G3P Dehydrogenases, and Glycerol Kinase Suggest Derived Features of Archaeal Membranes Having G1P Polar Lipids. Archaea 2016, 2016, 1802675. (d) Caforio, A.; Siliakus, M. F.; Exterkate, M.; Jain, S.; Jumde, V. R.; Andringa, R. L. H.; Kengen, S. W. M.; Minnaard, A. J.; Driessen, A. J. M.; van der Oost, J. Converting Escherichia Coli into an Archaebacterium with a Hybrid Heterochiral Membrane. Proc. Natl. Acad. Sci. U.S.A. 2018, 115, 3704-3709.

(6) (a) Bangham, A. D.; Horne, R. W. Negative Staining of Phospholipids and Their Structural Modification by Surface-Active Agents as Observed in the Electron Microscope. *J. Mol. Biol.* **1964**, *8*, 660–668. (b) Bangham, A. D.; Standish, M. M.; Watkins, J. C. Diffusion of Univalent Ions across the Lamellae of Swollen Phospholipids. *J. Mol. Biol.* **1965**, *13*, 238–252. (c) Seoane, A.; Brea, R. J.; Fuertes, A.; Podolsky, K. A.; Devaraj, N. K. Biomimetic Generation and Remodeling of Phospholipid Membranes by Dynamic

Imine Chemistry. J. Am. Chem. Soc. 2018, 140, 8388–8391. (d) Ringsdorf, H.; Schlarb, B.; Venzmer, J. Molecular Architecture and Function of Polymeric Oriented Systems: Models for the Study of Organization, Surface Recognition, and Dynamics of Biomembranes. Angew. Chem., Int. Ed. Engl. 1988, 27, 113–158. (e) Kunitake, T. Synthetic Bilayer Membranes: Molecular Design, Self-Organization, and Application. Angew. Chem., Int. Ed. Engl. 1992, 31, 709–726. (f) Brea, R. J.; Hardy, M. D.; Devaraj, N. K. Towards Self-Assembled Hybrid Artificial Cells: Novel Bottom-up Approaches to Functional Synthetic Membranes. Chem.—Eur. J. 2015, 21, 12564–12570. (g) Flores, J.; White, B. M.; Brea, R. J.; Baskin, J. M.; Devaraj, N. K. Lipids: Chemical Tools for Their Synthesis, Modification, and Analysis. Chem. Soc. Rev. 2020, 49, 4602–4614. (h) Podolsky, K. A.; Devaraj, N. K. Synthesis of Lipid Membranes for Artificial Cells. Nat. Rev. Chem. 2021, 5, 676–694.

(7) (a) Lasic, D. D.; Needham, D. The "Stealth" Liposome: A Prototypical Biomaterial. *Chem. Rev.* **1995**, 95, 2601–2628. (b) Immordino, M. L.; Dosio, F.; Cattel, L. Stealth Liposomes: Review of the Basic Science, Rationale, and Clinical Applications, Existing and Potential. *Int. J. Nanomed.* **2006**, 1, 297–315.

(8) (a) Discher, B. M.; Won, Y.-Y.; Ege, D. S.; Lee, J. C.-M.; Bates, F. S.; Discher, D. E.; Hammer, D. A. Polymersomes: Tough Vesicles Made from Diblock Copolymers. *Science* 1999, 284, 1143–1146. (b) Lee, J. S.; Feijen, J. Polymersomes for Drug Delivery: Design, Formation and Characterization. *J. Controlled Release* 2012, 161, 473–483. (c) Deming, T. J. Preparation and Development of Block Copolypeptide Vesicles and Hydrogels for Biological and Medical Applications. *Wiley Interdiscip. Rev.: Nanomed. Nanobiotechnol.* 2014, 6, 283–297.

(9) (a) Allen, T. M.; Cullis, P. R. Drug Delivery Systems: Entering the Mainstream. Science 2004, 303, 1818-1822. (b) Torchilin, V. P. Recent Advances with Liposomes as Pharmaceutical Carriers. Nat. Rev. Drug Discovery 2005, 4, 145-160. (c) de Jong, O. G.; Kooijmans, S. A. A.; Murphy, D. E.; Jiang, L.; Evers, M. J. W.; Sluijter, J. P. G.; Vader, P.; Schiffelers, R. M. Drug Delivery with Extracellular Vesicles: From Imagination to Innovation. Acc. Chem. Res. 2019, 52, 1761-1770. (d) EL Andaloussi, S.; Mäger, I.; Breakefield, X. O.; Wood, M. J. A. Extracellular Vesicles: Biology and Emerging Therapeutic Opportunities. Nat. Rev. Drug Discovery 2013, 12, 347-357. (e) Dong, Y.; Yu, T.; Ding, L.; Laurini, E.; Huang, Y.; Zhang, M.; Weng, Y.; Lin, S.; Chen, P.; Marson, D.; Jiang, Y.; Giorgio, S.; Pricl, S.; Liu, X.; Rocchi, P.; Peng, L. A Dual Targeting Dendrimer-Mediated SiRNA Delivery System for Effective Gene Silencing in Cancer Therapy. J. Am. Chem. Soc. 2018, 140, 16264-16274. (f) Lee, C. C.; MacKay, J. A.; Fréchet, J. M. J.; Szoka, F. C. Designing Dendrimers for Biological Applications. Nat. Biotechnol. 2005, 23, 1517-1526. (g) Tu, Y.; Peng, F.; Adawy, A.; Men, Y.; Abdelmohsen, L. K. E. A.; Wilson, D. A. Mimicking the Cell: Bio-Inspired Functions of Supramolecular Assemblies. Chem. Rev. 2016, 116, 2023-2078. (h) Thota, B. N. S.; Urner, L. H.; Haag, R. Supramolecular Architectures of Dendritic Amphiphiles in Water. Chem. Rev. 2016, 116, 2079-2102. (i) Weiss, M.; Frohnmayer, J. P.; Benk, L. T.; Haller, B.; Janiesch, J.-W.; Heitkamp, T.; Börsch, M.; Lira, R. B.; Dimova, R.; Lipowsky, R.; Bodenschatz, E.; Baret, J.-C.; Vidakovic-Koch, T.; Sundmacher, K.; Platzman, I.; Spatz, J. P. Sequential Bottom-up Assembly of Mechanically Stabilized Synthetic Cells by Microfluidics. Nat. Mater. 2018, 17, 89-96. (j) Gillies, E. R.; Frechet, J. M. J. Dendrimers and Dendritic Polymers in Drug Delivery. Drug Discovery Today 2005, 10, 35-43. (k) Dendrimers and Other Dendritic Polymers; Tomalia, D. A., Fréchet, J. M. J., Eds.; Wiley: Amsterdam, The Netherlands, 2001. (l) Esfand, R.; Tomalia, D. A. Poly-(Amidoamine) (PAMAM) Dendrimers: From Biomimicry to Drug Delivery and Biomedical Applications. Drug Discovery Today 2001, 6, 427-436. (m) Svenson, S.; Tomalia, D. A. Dendrimers in Biomedical Applications-Reflections on the Field. Adv. Drug Delivery Rev. 2005, 57, 2106-2129. (n) Thota, N. S.; Urner, L. H.; Haag, R. Supramolecular Architectures of Dendritic Amphiphiles in Water. Chem. Rev. 2016, 116, 2079-2102. (o) Calderón, M.; Quadir, M. A.; Sharma, S. K.; Haag, R. Dendritic Polyglycerol for Biomedical

Applications. Adv. Mater. 2010, 22, 190–218. (p) Khandare, J.; Calderón, M.; Dagia, N. M.; Haag, R. Multifunctional Dendritic Polymers in Nanomedicine: Opportunities and Challenges. Chem. Soc. Rev. 2012, 41, 2824–2848. (q) Bellomo, E. G.; Wyrsta, M. D.; Pakstis, L.; Pochan, D. J.; Deming, T. J. Stimuli-Responsive Polypeptide Vesicles by Conformation-Specific Assembly. Nat. Mater. 2004, 3, 244–248. (r) Pelegri-O'Day, E. M.; Lin, E.-W.; Maynard, H. D. Therapeutic Protein-Polymer Conjugates: Advancing Beyond PEGylation. J. Am. Chem. Soc. 2014, 136, 14323–14332.

(10) (a) Percec, V.; Wilson, D. A.; Leowanawat, P.; Wilson, C. J.; Hughes, A. D.; Kaucher, M. S.; Hammer, D. A.; Levine, D. H.; Kim, A. J.; Bates, F. S.; Davis, K. P.; Lodge, T. P.; Klein, M. L.; DeVane, R. H.; Agad, E.; Rosen, B. M.; Argintaru, A. O.; Sienkowska, M. J.; Rissanen, K.; Nummelin, S.; Ropponen, J. Self-Assembly of Janus Dendrimers into Uniform Dendrimersomes and Other Complex Architectures. Science 2010, 328, 1009-1014. (b) Percec, V.; Leowanawat, P.; Sun, H.-J.; Kulikov, O.; Nusbaum, C. D.; Tran, T. M.; Bertin, A.; Wilson, D. A.; Peterca, M.; Zhang, S.; Kamat, N. P.; Vargo, K.; Moock, D.; Johnston, E. D.; Hammer, D. A.; Pochan, D. J.; Chen, Y.; Chabre, Y. M.; Shiao, T. C.; Bergeron-Brlek, M.; André, S.; Roy, R.; Gabius, H.-J.; Heiney, P. A. Modular Synthesis of Amphiphilic Janus Glycodendrimers and Their Self-Assembly into Glycodendrimersomes and Other Complex Architectures with Bioactivity to Biomedically Relevant Lectins. J. Am. Chem. Soc. 2013, 135, 9055-9077. (c) Xiao, Q.; Rubien, J. D.; Wang, Z.; Reed, E. H.; Hammer, D. A.; Sahoo, D.; Heiney, P. A.; Yadavalli, S. S.; Goulian, M.; Wilner, S. E.; Baumgart, T.; Vinogradov, S. A.; Klein, M. L.; Percec, V. Self-Sorting and Coassembly of Fluorinated, Hydrogenated, and Hybrid Janus Dendrimers into Dendrimersomes. J. Am. Chem. Soc. 2016, 138, 12655-12663. (d) Rodriguez-Emmenegger, C.; Xiao, Q.; Kostina, N. Y.; Sherman, S. E.; Rahimi, K.; Partridge, B. E.; Li, S.; Sahoo, D.; Reveron Perez, A. M.; Buzzacchera, I.; Han, H.; Kerzner, M.; Malhotra, I.; Möller, M.; Wilson, C. J.; Good, M. C.; Goulian, M.; Baumgart, T.; Klein, M. L.; Percec, V. Encoding Biological Recognition in a Bicomponent Cell-Membrane Mimic. Proc. Natl. Acad. Sci. U.S.A. 2019, 116, 5376-5382. (e) Sherman, S. E.; Xiao, Q.; Percec, V. Mimicking Complex Biological Membranes and Their Programmable Glycan Ligands with Dendrimersomes and Glycodendrimersomes. Chem. Rev. 2017, 117, 6538-6631. (f) Peterca, M.; Percec, V.; Leowanawat, P.; Bertin, A. Predicting the Size and Properties of Dendrimersomes from the Lamellar Structure of Their Amphiphilic Janus Dendrimers. J. Am. Chem. Soc. 2011, 133, 20507-20520. (g) Buzzacchera, I.; Xiao, Q.; Han, H.; Rahimi, K.; Li, S.; Kostina, N. Y.; Toebes, B. J.; Wilner, S. E.; Möller, M.; Rodriguez-Emmenegger, C.; Baumgart, T.; Wilson, D. A.; Wilson, C. J.; Klein, M. L.; Percec, V. Screening Libraries of Amphiphilic Janus Dendrimers based on Natural Phenolic Acids to Discover Monodisperse Unilamellar Dendrimersomes. Biomacromolecules 2019, 20, 712-727.

(11) (a) Torre, P.; Xiao, Q.; Buzzacchera, I.; Sherman, S. E.; Rahimi, K.; Kostina, N. Y.; Rodriguez-Emmenegger, C.; Möller, M.; Wilson, C. J.; Klein, M. L.; Good, M. C.; Percec, V. Encapsulation of Hydrophobic Components in Dendrimersomes and Decoration of Their Surface with Proteins and Nucleic Acids. Proc. Natl. Acad. Sci. U.S.A. 2019, 116, 15378-15385. (b) Yadavalli, S. S.; Xiao, Q.; Sherman, S. E.; Hasley, W. D.; Klein, M. L.; Goulian, M.; Percec, V. Bioactive Cell-Like Hybrids from Dendrimersomes with a Human Cell Membrane and Its Components. Proc. Natl. Acad. Sci. U.S.A. 2019, 116, 744-752. (c) Xiao, Q.; Delbianco, M.; Sherman, S. E.; Reveron Perez, A. M.; Bharate, P.; Pardo-Vargas, A.; Rodriguez-Emmenegger, C.; Kostina, N. Y.; Rahimi, K.; Söder, D.; Möller, M.; Klein, M. L.; Seeberger, P. H.; Percec, V. Nanovesicles Displaying Functional Linear and Branched Oligomannose Self-Assembled from Sequence-Defined Janus Glycodendrimers. Proc. Natl. Acad. Sci. U.S.A. 2020, 117, 11931-11939. (d) Li, S.; Xia, B.; Javed, B.; Hasley, W. D.; Melendez-Davila, A.; Liu, M.; Kerzner, M.; Agarwal, S.; Xiao, Q.; Torre, P.; Bermudez, J. G.; Rahimi, K.; Kostina, N. Y.; Möller, M.; Rodriguez-Emmenegger, C.; Klein, M. L.; Percec, V.; Good, M. C. Direct Visualization of Vesicle Disassembly and Reassembly Using

Photocleavable Dendrimers Elucidates Cargo Release Mechanisms. ACS Nano 2020, 14, 7398-7411.

- (12) Xiao, Q.; Ludwig, A.-K.; Romanò, C.; Buzzacchera, I.; Sherman, S. E.; Vetro, M.; Vértesy, S.; Kaltner, H.; Reed, E. H.; Möller, M.; Wilson, C. J.; Hammer, D. A.; Oscarson, S.; Klein, M. L.; Gabius, H.-J.; Percec, V. Exploring Functional Pairing between Surface Glycoconjugates and Human Galectins Using Programmable Glycodendrimersomes. *Proc. Natl. Acad. Sci. U.S.A.* **2018**, *115*, E2509—E2518.
- (13) (a) Zhang, D.; Atochina-Vasserman, E. N.; Maurya, D. S.; Huang, N.; Xiao, Q.; Ona, N.; Liu, M.; Shahnawaz, H.; Ni, H.; Kim, K.; Billingsley, M. M.; Pochan, D. J.; Mitchell, M. J.; Weissman, D.; Percec, V. One-Component Multifunctional Sequence-Defined Ionizable Amphiphilic Janus Dendrimer Delivery Systems for mRNA. J. Am. Chem. Soc. 2021, 143, 12315-12327. (b) Zhang, D.; Atochina-Vasserman, E. N.; Maurya, D. S.; Liu, M.; Xiao, Q.; Lu, J.; Lauri, G.; Ona, N.; Reagan, E. K.; Ni, H.; Weissman, D.; Percec, V. Targeted Delivery of mRNA with One-Component Ionizable Amphiphilic Janus Dendrimers. J. Am. Chem. Soc. 2021, 143, 17975-17982. (c) Zhang, D.; Atochina-Vasserman, E. N.; Lu, J.; Maurya, D. S.; Xiao, Q.; Liu, M.; Adamson, J.; Ona, N.; Reagan, E. K.; Ni, H.; Weissman, D.; Percec, V. The Unexpected Importance of the Primary Structure of the Hydrophobic Part of One-Component Ionizable Amphiphilic Janus Dendrimers in Targeted mRNA Delivery Activity. J. Am. Chem. Soc. 2022, 144, 4746-4753.
- (14) (a) Zhang, S.; Sun, H.-J.; Hughes, A. D.; Moussodia, R.-O.; Bertin, A.; Chen, Y.; Pochan, D. J.; Heiney, P. A.; Klein, M. L.; Percec, V. Self-Assembly of Amphiphilic Janus Dendrimers into Uniform Onion-Like Dendrimersomes with Predictable Size and Number of Bilayers. Proc. Natl. Acad. Sci. U.S.A. 2014, 111, 9058-9063. (b) Zhang, S.; Sun, H.-J.; Hughes, A. D.; Draghici, B.; Lejnieks, J.; Leowanawat, P.; Bertin, A.; Otero De Leon, L.; Kulikov, O. V.; Chen, Y.; Pochan, D. J.; Heiney, P. A.; Percec, V. "Single-Single" Amphiphilic Janus Dendrimers Self-Assemble into Uniform Dendrimersomes with Predictable Size. ACS Nano 2014, 8, 1554-1565. (c) Zhang, S.; Xiao, Q.; Sherman, S. E.; Muncan, A.; Ramos Vicente, A. D. M.; Wang, Z.; Hammer, D. A.; Williams, D.; Chen, Y.; Pochan, D. J.; Vértesy, S.; André, S.; Klein, M. L.; Gabius, H.-J.; Percec, V. Glycodendrimersomes from Sequence-Defined Janus Glycodendrimers Reveal High Activity and Sensor Capacity for the Agglutination by Natural Variants of Human Lectins. J. Am. Chem. Soc. 2015, 137, 13334-13344. (d) Xiao, Q.; Zhang, S.; Wang, Z.; Sherman, S. E.; Moussodia, R.-O.; Peterca, M.; Muncan, A.; Williams, D. R.; Hammer, D. A.; Vértesy, S.; André, S.; Gabius, H.-J.; Klein, M. L.; Percec, V. Onion-Like Glycodendrimersomes from Sequence-Defined Janus Glycodendrimers and Influence of Architecture on Reactivity to a Lectin. Proc. Natl. Acad. Sci. U.S.A. 2016, 113, 1162-1167. (e) Kostina, N. Y.; Wagner, A. M.; Haraszti, T.; Rahimi, K.; Xiao, Q.; Klein, M. L.; Percec, V.; Rodriguez-Emmenegger, C. Unraveling Topology-Induced Shape Transformations in Dendrimersomes. Soft Matter 2021, 17, 254-267. (f) Joseph, A.; Wagner, A. M.; Garay-Sarmiento, M.; Aleksanyan, M.; Haraszti, T.; Söder, D.; Georgiev, V. N.; Dimova, R.; Percec, V.; Rodriguez-Emmenegger, C. Zwitterionic Dendrimersomes: A Closer Xenobiotic Mimic of Cell Membranes. Adv. Mater. 2022, 34, 2206288.
- (15) (a) Shinoda, W.; DeVane, R.; Klein, M. L. Zwitterionic Lipid Assemblies: Molecular Dynamics Studies of Monolayers, Bilayers, and Vesicles Using a New Coarse Grain Force Field. *J. Phys. Chem. B* **2010**, 114, 6836–6849. (b) Shinoda, W.; DeVane, R.; Klein, M. L. Coarse-Grained Molecular Modeling of Non-Ionic Surfactant Self-Assembly. Soft Matter **2008**, 4, 2454–2462. (c) Shinoda, W.; DeVane, R.; Klein, M. L. Computer Simulation Studies of Self-Assembling Macromolecules. Curr. Opin. Struct. Biol. **2012**, 22, 175–186. (d) Seo, S.; Shinoda, W. SPICA Force Field for Lipid Membranes: Domain Formation Induced by Cholesterol. *J. Chem. Theory Comput.* **2019**, 15, 762–774.
- (16) (a) Walde, P.; Wick, R.; Fresta, M.; Mangone, A.; Luisi, P. L. Autopoietic Self-Reproduction of Fatty Acid Vesicles. *J. Am. Chem. Soc.* 1994, 116, 11649–11654. (b) Szostak, J. W.; Bartel, D. P.; Luisi,

- P. L. Synthesizing life. *Nature* **2001**, 409, 387–390. (c) Blain, J. C.; Szostak, J. W. Progress Toward Synthetic Cells. *Annu. Rev. Biochem.* **2014**, 83, 615–640. (d) Kindt, J. T.; Szostak, J. W.; Wang, A. Bulk Self-Assembly of Giant, Unilamellar Vesicles. *ACS Nano* **2020**, 14, 14627–14634.
- (17) (a) Rosen, B. M.; Peterca, M.; Morimitsu, K.; Dulcey, A. E.; Leowanawat, P.; Resmerita, A. M.; Imam, M. R.; Percec, V. Programming the Supramolecular Helical Polymerization of Dendritic Dipeptides via the Stereochemical Information of the Dipeptide. J. Am. Chem. Soc. 2011, 133, 5135-5151. (b) Percec, V.; Dulcey, A. E.; Balagurusamy, V. S. K.; Miura, Y.; Smidrkal, J.; Peterca, M.; Nummelin, S.; Edlund, U.; Hudson, S. D.; Heiney, P. A.; Duan, H.; Magonov, S. N.; Vinogradov, S. A. Self-Assembly of Amphiphilic Dendritic Dipeptides into Helical Pores. Nature 2004, 430, 764-768. (c) Kaucher, M. S.; Peterca, M.; Dulcey, A. E.; Kim, S. A.; Vinogradov, D. A.; Hammer, P. A.; Heiney, V.; Percec, V. Selective Transport of Water Mediated by Porous Dendritic Dipeptides. J. Am. Chem. Soc. 2007, 129, 11698-11699. (d) Rosen, B. M.; Roche, C.; Percec, V. Self-Assembly of Dendritic Dipeptides as a Model for Chiral Selection of Promitive Biological Systems. Top. Curr. Chem. 2013, 333, 213-253. (e) Percec, V.; Leowanawat, P. Why Are Biological Systems Homochiral? Isr. J. Chem. 2011, 51, 1107-1117. (f) Percec, V.; Xiao, Q. Helical Chirality of Supramolecular Columns and Speres Self-Organizes Complex Liquid Crystals, Crystals, and Quasicrystals. Isr. J. Chem. 2021, 61, 530-556. (g) Percec, V.; Xiao, Q. Helical Self-Organizations and Emerging Functions in Architectures, Biological and Synthetic Macromolecules. Bull. Chem. Soc. Jpn. 2021, 94, 900-928.
- (18) (a) Roche, C.; Sun, H.-J.; Prendergast, M. E.; Leowanawat, P.; Partridge, B. E.; Heiney, P. A.; Araoka, F.; Graf, R.; Spiess, R. W.; Zeng, H. B. O.; Ungar, G.; Percec, V. Homochiral Columns Constructed by Chiral Self-Sorting During Supramolecular Helical Organization of Hat-Shaped Molecules. *J. Am. Chem. Soc.* 2014, 136, 7169–7185. (b) Roche, C.; Sun, H.-J.; Leowanawat, P.; Araoka, F.; Partridge, B. E.; Peterca, M.; Wilson, D. A.; Prendergast, M. E.; Heiney, P. A.; Graf, R.; Spiess, R. W.; Zeng, H. B. O.; Ungar, G.; Percec, V. A Supramolecular Helix that Disregards Chirality. *Nat. Chem.* 2016, 8, 80–89.
- (19) (a) Arai, N.; Yasuoka, K.; Zeng, X. C. Self-Assembly of Janus Oligomers into Onion-Like Vesicles with Layer-by-Layer Water Discharging Capability: A Minimalist Model. *ACS Nano* **2016**, *10*, 8026–8037. (b) Hu, F.-F.; Sun, Y.-W.; Zhu, Y.-L.; Huang, Y.-N.; Li, Z.-W.; Sun, Z.-Y. Enthalpy-Driven Self-Assembly of Amphiphilic Janus Dendrimers into Onion-Like Vesicles: A Janus Particle Model. *Nanoscience* **2019**, *11*, 17350–17356.